Computational model for nuclear reaction studies: Quasiparticle dynamics

David H. Boal and James N. Glosli
TRIUMF, Vancouver, British Columbia, Canada V6T 2A3
and Department of Physics, Simon Fraser University, Burnaby, British Columbia, Canada V5A 1S6
(Received 25 July 1988)

A computation model for nuclear reaction studies which is based upon a momentum dependent interaction between quasiparticles is extended to include collisions between the nucleons. The model is first used to examine the time scales involved in fragment formation at intermediate energies, both as a function of bombarding energy and impact parameter. The distribution of excitation energies and angular momenta of the reaction products is also investigated since the model possesses stable ground states. Several reactions are chosen as examples: Ar+C at 12A MeV, and Ca+Ca at 25A, 50A, and 100A MeV. The time scale for changes in mass distribution, etc., is discussed and the need for an afterburner scheme is established.

I. INTRODUCTION

Recently, we[1] proposed a computational model for nucleon interactions that incorporated some of the effects of antisymmetrization through the use of a momentum dependent potential. The motivation for this approach was to be able to replace a completely antisymmetrized many-body wave function with a simple product state of single-particle wave functions. We choose Gaussian wave packets with a fixed width parameter for the single-particle states, such that the many-body wave function is represented at all times as

$$\psi(r_1,\ldots,r_n,t)=\prod_{i=1}^{n}\frac{\exp\left[-\frac{\alpha^2}{2}[\mathbf{r}_i-\mathbf{R}_i(t)]^2\right]}{N_i}\exp[i\mathbf{P}_i(t)\cdot\mathbf{r}_i]\chi_i^I\chi_i^S\,, \tag{1}$$

where $R_i(t)$ and $P_i(t)$ are the expectations of the position and momentum of the ith particle at time t and N_i is the normalization factor of the ith particle. The isospin and spin wave functions are labeled by χ^I and χ^S. In this model, the degrees of freedom necessary to describe the system are reduced to the set of phase space coordinates R_i,P_i. The evolution of the system of nucleons is represented by a collection of quasiparticles obeying classical equations of motion.

The form of the momentum dependent potential was arrived at by evaluating the kinetic energy of a pair of identical particles with antisymmetrized Gaussian wave functions. The candidate potential has the form

$$V_p(X_{ab})=V_s\frac{\alpha^2\hbar^2X_{ab}}{2m\,(e^{X_{ab}}-1)}\,, \tag{2}$$

where

$$X_{ab}=\tfrac{1}{2}[\alpha^2(\mathbf{R}_a-\mathbf{R}_b)^2+(\mathbf{P}_a-\mathbf{P}_b)^2/(\hbar^2\alpha^2)]$$

and V_s is a parameter. This potential, when applied pairwise to a many-body system has the interesting property that the ground state changes from a zero kinetic energy state at low density to a finite kinetic energy state as the density is increased. This behavior arises because the potential is always repulsive and the length scale of the potential is the separation of the particles in phase space. Hence, the closer the quasiparticles are placed in position space the more they will be forced apart in momentum space.

The ground-state properties of nuclei were investigated by adding to the Pauli potential a density dependent potential representing the nuclear interaction. In Ref. 1 it was shown that the binding energies and rms radii of the computational nuclei agreed with the observed values over a wide mass range at the level of a few tenths of an MeV per nucleon and a few tenths of a Fermi, respectively.

In Ref. 1, it was not necessary to determine the dynamics of the quasiparticles, since the nuclear ground-state properties depend only on the Hamiltonian of the system. In this paper, we wish to formulate a prescription of the dynamics so as to be able to apply the model to reactions. We will refer to this quasiparticle model, including the collision prescription, as Quasiparticle Dynamics or (QPD). The purpose of the following section of the paper, then, is to obtain a method of incorporating the dynamics which has some aspects of quantum mechanics, yet at the same time conserves angular momentum. In Sec. III, the model is used to study the time scales involved in the thermalization stages of intermediate energy reactions, as a function of both bombarding energy and impact parameter. Because QPD contains proper ground states, it can be used to investigate excitation en-

ergy and angular momentum distributions, and this is done in Sec. IV. This section also establishes the need for an afterburner code to follow evaporative decays if detailed comparisons are to be made with experiment.

II. *NN* COLLISIONS

In previous studies[2] of the dynamics of heavy-ion reactions, it was found that the collisionless Boltzmann equation underestimated the magnitude of the cross section. That is, replacing the nuclear interaction by a simple density dependent mean field resulted in nuclei with too much transparency at intermediate bombarding energies. The incorporation of a collision term in this kinetic equation appears to provide a much better description of the reaction dynamics.

In Ref. 1, a density dependent potential was used along with the Pauli potential to determine the energetics of nuclear binding. Because the quasiparticles are stationary in the ground state, collisions will not effect ground-state properties and so we made no attempt to incorporate collisions in Ref. 1. However, to apply the model to nuclear reactions, it is likely that a collision term must be included in it just as in the Boltzmann equation approach.

We begin our discussion of the collision term with a description of one of the techniques commonly used for incorporating it in the Boltzmann equation approaches [which we refer to as Nordheim-Uehling-Uhlenbeck[3] or (NUU)]. Two ingredients are needed: a definition of when the collision occurs, and a prescription for determining the new momenta of the pair of interacting particles after scattering has occurred. The distance of closest approach is often used to define the collision point. The new momenta are then chosen stochastically according to a distribution governed by the observed scattering cross section. This procedure can be made to conserve energy and linear momentum, but not necessarily angular momentum. The difficulty with angular momentum conservation lies in the fact that the relation between impact parameter and scattering angle has been given up in adopting the stochastic scattering procedure.

We wish to introduce scattering into our model in terms of stochastic hard-sphere scattering between quasiparticles. Since the quasiparticles behave as classical particles, if they scatter, their change of momentum can be calculated from the conservation laws and is unique. This change needs to be calculated numerically because of the momentum dependent potential in our model.

Computationally, we can solve for the new momenta of the colliding particles, say particles 1 and 2 in the following way. From conservation of linear and angular momentum we can write that

$$\mathbf{P}_1'=\mathbf{P}_1+\Delta\hat{\mathbf{X}}_{12},\quad \mathbf{P}_2'=\mathbf{P}_2-\Delta\hat{\mathbf{X}}_{12}\ , \tag{3}$$

where $\mathbf{P}_i$ is the old momentum, P_i' is the new momentum, $\hat{\mathbf{X}}_{12}$ is the unit vector along the $\mathbf{X}_1-\mathbf{X}_2$ direction and the scalar Δ is to be determined from conservation of energy. From conservation of energy we can write that the change of energy must vanish:

$$E'-E=\frac{(\mathbf{P}_1-\mathbf{P}_2)\cdot\hat{\mathbf{X}}_{12}\Delta+\Delta^2}{m}+V(X_1,\ldots,X_n,\mathbf{P}_1+\Delta X_{12},\mathbf{P}_2-\Delta\hat{\mathbf{X}}_{12},\mathbf{P}_3,\ldots,\mathbf{P}_n)$$
$$-V(X_1,\ldots,X_n,\mathbf{P}_1,\mathbf{P}_2,\mathbf{P}_3,\ldots,\mathbf{P}_n)=0\ . \tag{4}$$

Notice that Eq. (4) has at least one solution, the trivial solution $\Delta=0$. To find the nonzero roots of (4) we use the secant method to solve the equation,

$$\frac{(\mathbf{P}_1-\mathbf{P}_2)\cdot X_{12}+\Delta}{m}+\frac{1}{\Delta}[V(\mathbf{P}_1+\Delta X_{12},\mathbf{P}_2-\Delta\hat{\mathbf{X}}_{12},\ldots,)-V(\mathbf{P}_1,\mathbf{P}_2,\ldots,)]=0\ , \tag{5}$$

using as an initial guess for the solution the value of Δ for scattering without the Pauli term.

In general, it takes less than 10 iterations to find the solution. Obviously, if the procedure fails to yield anything other than the trivial solution because of the presence of the Pauli potential (the nuclear potential energy does not change since it is position dependent only), then the collision is rejected.

To make the scattering nondeterministic we choose stochastically between the scattered and unscattered state at each time step in the calculation. The stochastic scheme involves assigning one test particle to each quasiparticle according to the Gaussian density distribution of the quasiparticle. If the distance between test particles associated with a quasiparticle pair falls below a given value the trial scattered state is accepted and new test particle positions are assigned to the scattered quasiparticle pair.

The magnitude of the radius used to set the threshold for test particle scattering we determine from the total *NN* cross section, which we take to be equal to 28 mb for both identical and nonidentical particle pairs.[4] (We arrived at this value in an analysis of data summarized in Ref. 4.) The observed differential cross section is roughly isotropic. In the limit when the wave packet width parameter α goes to infinity, that is the wave packets become pointlike, then this procedure reproduces hard-sphere scattering. For small α, the predicted angular distributions are no longer isotropic, however, even though the total cross section remains the same. For $\alpha=0.5$ fm^{-1}, the value that we chose in Ref. 1, the predicted differential cross section for *NN* scattering is shown in Fig. 1. The ragged shape to the cross section arises from the integration procedure: The differential cross section was simulated at 0.5 fm steps in the impact parameter, with 4000 events per impact parameter. Because of the

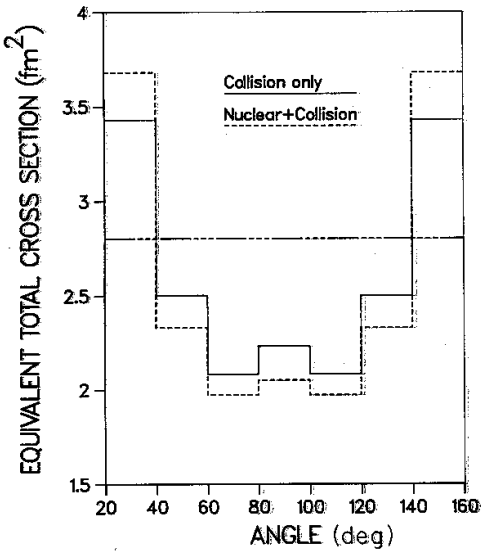

FIG. 1. Associated total NN cross section in the model for $=0.5$ fm^{-1}. The cross section was calculated by taking the simulated differential cross section at each angle and assuming isotropy. The full curve is from the scattering term only, while the dashed curve includes the scattering term plus the nuclear potential.

multiple scattering present in the reactions of interest to us, the deviation from isotropy associated with this prescription is of little significance.

One new momenta have been chosen for the scattering pair, a test is made for Pauli blocking. To determine the probability that the collision is not Pauli blocked, Wigner transforms[5] are used to go over to a phase space description of the system. The phase space distribution of a single particle is given by

$$f_i(r,p)=\frac{1}{(\pi\hbar)^3}e^{-[\alpha^2(\mathbf{r}-\mathbf{R}_i)^2+(\mathbf{p}+\mathbf{P}_i)^2/\alpha^2\hbar^2]} . \tag{6}$$

The density function for particles of a specific I,S combination is given by [consistent with Eq. (1)]:

$$f_T^{IS}(r,p)=\sum_{i=1}^{n} f_i(r,p)\delta_{I,I_i}\delta_{S,S_i} . \tag{7}$$

Now consider the scattering of particle 1 where f'_1 is its new phase space distribution after scattering. If we divide phase space into cells of volume $(2\pi\hbar)^3$ then the collision will be Pauli blocked if particle 1 is scattered into a cell occupied by a particle with the same quantum numbers I,S.

The probability that a cell is occupied by some particle other than particle 1 but sharing the same I and S as particle 1 is

$$P_{\text{occupied}}(r,p)=(2\pi\hbar)^3(f_T^{IS}-f_1) , \tag{8}$$

where we have assumed that f_T-f_1 is slowly varying in phase space in the vicinity of r,p.

The probability that the scattering of particle 1 is blocked is then given by

$$\begin{aligned}P^1_{\text{blocked}}&=\int f'_1(r,p)P_{\text{occupied}}(r,p)d^3rd^3p\\&=(2\pi\hbar)^2\sum_{i\neq 1}\delta_{II_i}\delta_{SS_i}\int f'_1(r,p)f_i(r,p)d^3rd^3p\\&=\sum_{i\neq 1}\delta_{II_i}\delta_{SS_i}\exp\{-\tfrac{1}{2}[\alpha^2(\mathbf{R}'_1-\mathbf{R}_i)^2+(\mathbf{P}'_1-\mathbf{P}_i)^2/\alpha^2\hbar^2]\} .\end{aligned} \tag{9}$$

Likewise, we can calculate the blocking probability, P^2_{blocked}, for the scattering of the other member of the scattering pair, particle 2. The probability that a collision is accepted is then the probability that particle 1 and particle 2 are not blocked, or

$$P_{\text{accept}}=(1-P^1_{\text{blocked}})(1-P^2_{\text{blocked}}) . \tag{10}$$

Because of the approximations made in this calculation, we do not reproduce the Fermion probabilities completely faithfully. In particular, this procedure may lead to configurations in which phase space saturation is exceeded (a problem which this model shares with NUU models). If P_{blocked} exceeds unity due to the oversaturation we artificially set it to unity in the calculation.

The test particle method is not the only one to come to mind for handling the collision term, of course. Other possibilities include:

(i) using the same test particle technique as outlined earlier but generating a new set of test particles after each time step instead of after each collision.

(ii) avoiding test particles completely by comparing quasiparticle separations at each time step with an algorithm which determines (in a stochastic manner) whether a collision takes place.

We felt that neither of these approaches was simpler to implement than the one chosen here. Probably a more important extension to the algorithm we propose would be to replace the hard-sphere geometry of the test particle interaction with a different geometrical shape: that is, make the scattering radius depend on impact parameter. This would allow one to more accurately reproduce the differential cross section in free NN scattering, although

we doubt that this would make any significant difference to the simulation of heavy-ion reactions.

III. REACTION TIME SCALES

In a previous work,[6] we began an investigation of the different conditions produced in central versus peripheral collisions. The only observable we were able to predict was the mass yield curve, which showed significant impact parameter dependence. The limiting feature of the semiclassical equations of motion (SCEOM) model used in that investigation [which also applies to other models in the same class as SCEOM, for example, the quantum molecular dynamics (QMD) model[7]] is that the initial configurations used for the nuclei are not true ground states of the interaction used to propagate them. Unlike the molecular dynamics simulations used in the study of argon droplets[8] for example, these models cannot be used to calculate excitation energies or angular momenta of the fragments produced in a reaction. This may be particularly important for the study of low-energy, peripheral or proton induced reactions which only involve small excitation energies. The QPD model does not suffer from these difficulties.

In order to investigate the time scales involved in different reaction processes, several sample systems were simulated. The Ca+Ca reaction at 25A MeV and impact parameter, b, equal to 0, 3, and 6 fm and the Ca+Ca reaction at 50 and 100A MeV and $b=3$ fm, were chosen to span the intermediate energy region. For comparison with processes in the fusion regime, the Ar+C reaction[9] at 12A MeV and $b=2$, 4, and 6 fm was simulated. A sample of 500 events per impact parameter was generated for the Ca reactions, 250 events per impact parameter for the Ar+C reactions. On an IBM 3081 processor, a Ca+Ca event took approximately 1 cpu min to execute, for a reaction time of 250 fm/c. The execution time scales roughly with linearly with the reaction time, but as the square of the number of particles. The reader is directed to Ref. 1 for further details of the procedures used.

We begin with the Ca+Ca reaction at 25A MeV. Every 10 fm/c, the positions and momenta of the nucleons were written out to storage, and these were later run through a cluster search routine, which linked together nucleons which were separated in space by less than 3.5 fm. The time dependence of the cluster yield is shown in Fig. 2 for three mass bins: 1–10, 31–40, and 71–80. The upper part of the figure shows the results for $b=0$ while the bottom half is for $b=6$ fm.

In the peripheral collision, one can see that the nuclei join to form a large system, but this system does not fuse. The mass 31–40 bin, which initially contains two nuclei corresponding to the projectile and target, empties as the mass 71–80 bin fills. However, this large system subsequently breaks apart into a pair of nuclei very close in mass to Ca, with little exchange of energy, on the average, between the partners. This can be contrasted with the behavior of the central collision, where a highly excited system of nucleons is formed. This system decays with time, but does not break apart as the large system did in the peripheral collision. Further evidence on the relative

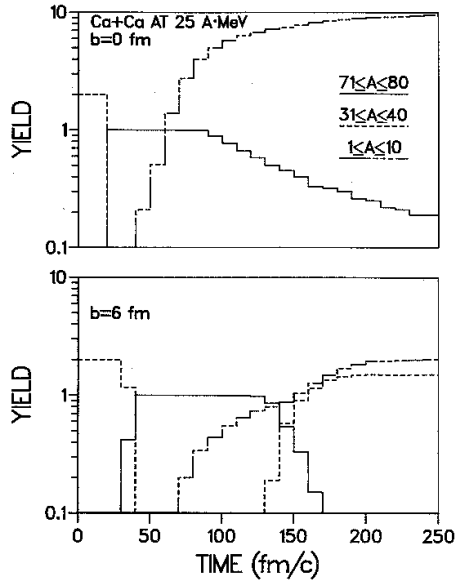

FIG. 2. Time dependence of the fragment mass distribution in the Ca+Ca reaction at 25A MeV for $b=0$ fm (top) and $b=6$ fm (bottom). Three mass bins are used in the figure, 1–10, 31–40, and 71–80 mass units.

excitation of the system can be found by examining the light fragment yield at the two impact parameters: There are five times as many light fragments and nucleons produced at $b=0$ fm than there are at $b=6$ fm.

This conclusion can be strengthened by examining the time dependence of the rms radii of the group of nucleons which emerge as a fragment. The technique is the following: As with Fig. 2, the positions of the nucleons are stored every 10 fm/c in the simulation. Then a cluster search is made over the final positions after an elapsed time of 150 fm/c and it is determined which nucleons belong to what clusters. The rms radius of a given cluster is determined by tracing its constituent nucleons through the reaction. The time scale of 150 fm/c was chosen so that $A=80$ systems were still present in the peripheral collision.

The results are shown in Fig. 3 for the same reactions as in Fig. 2. Turning first to the peripheral collision in the lower part of the figure, the rms radii are displayed for several different cluster masses. The radius of the $A=76$ system is necessarily large at first, since its nucleons are spread over both the projectile and the target. The radius shrinks as the nuclei approach and touch, then increases as they pass by each other. In contrast, in the central collision the increase after contact is much slower and tends towards a constant. The fact that there is little thermalization in the peripheral collisions can also be seen by looking at systems near $A=40$. Here, one expects few nucleon transfer to be important and this is what the simulation indicates. Nucleons which emerge in a fragment slightly larger than $A=40$ must be at least partly spread over the projectile and target (yielding a larger initial rms radius), while those which emerge in a

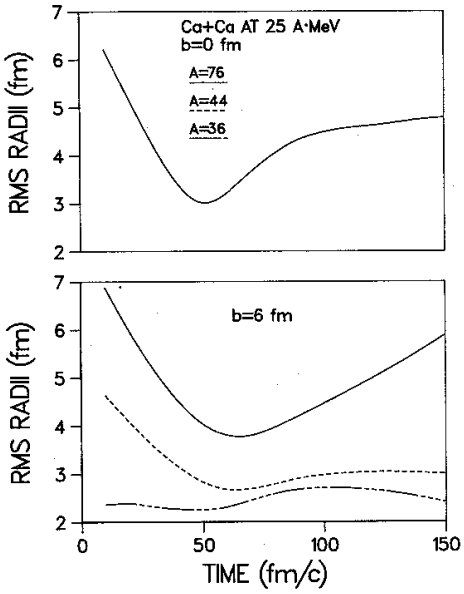

FIG. 3. Time dependence of the rms radii of nucleon positions for the Ca+Ca reaction at 25A MeV for $b=0$ fm (top) and $b=6$ fm (bottom). Three masses are chosen for display: 36, 44, and 76. See the text for a description of how the radii were determined.

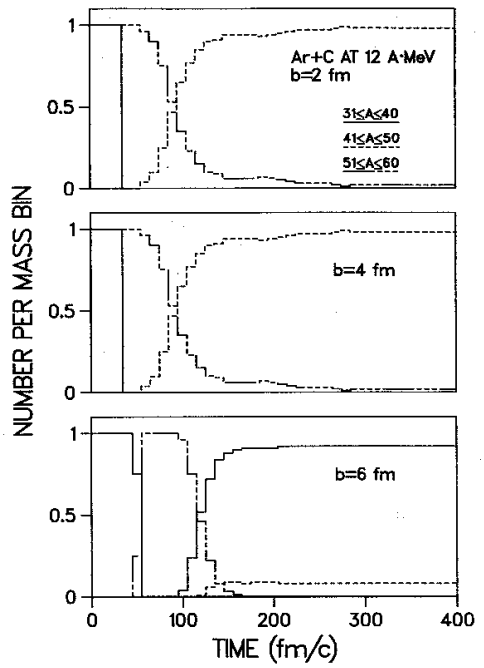

FIG. 4. Time dependence of the fragment mass distribution in the Ar+C reaction at 12A MeV for $b=2$ (top), 4 (middle) and 6 (bottom) fm. Three mass bins are used in the figure, 31–40, 41–50, and 51–60 mass units.

system somewhat smaller than $A=40$ are predominantly in one nucleus initially.

This situation can be contrasted with that which prevails at lower energies. The time evolution of the mass distribution in the Ar+C reaction at 12A MeV is shown in Fig. 4. The peripheral reaction (lower part of the figure) shows the same behavior as the Ca+Ca reactions of Fig. 2: the projectile and target link together to form a loose system which rapidly splits. However, the more "central" collisions lead to excited systems which fuse and then lose a few particles. Further, the relative yields do not have a strong impact parameter dependence (on the time scale of a few hundred fm/c) for $b<4$ fm. This general behavior is what one expects in this energy regime (see Ref. 10 and references therein, for example) although this model should not necessarily be expected to be a good tool for investigating fusion processes.

To complete our investigation of the time scales of these processes, we turn to characterizing nucleon emission. The quantity of interest is the particle emission rate. There are several possible definitions of emission time which could be used; the procedure which is used here is to follow the local density in the environment of a nucleon and find when it first falls below a fixed threshold, chosen to be 0.07 fm^{-3}. The time dependence of the emission rate so defined is shown in Fig. 5. For both of the impact parameters shown (Ca+Ca at 25A MeV, $b=0,6$ fm) the emission rate increases as the nuclei overlap and then decays exponentially after the time of maximum overlap. The integral of the emission is rate is obviously higher for the central collision, corresponding to the larger multiplicity expected with greater energy deposition.

Further, if one takes the slope of the semilog plot to determine an emission lifetime, one sees that there is a

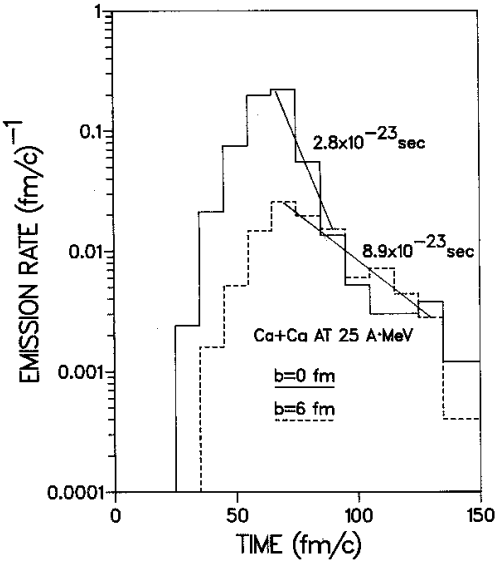

FIG. 5. Time dependence of nucleon emission rates for the two reactions of Fig. 2. A nucleon is considered to be "emitted" when the average local density around it falls below 0.07 fm^{-3} for the first time.

short lifetime component (3×10^{-23} sec) associated with the central collision which is not present in the peripheral one. There is also a longer lifetime component (9×10^{-23} sec) present in both reactions, although this component does not correspond to evaporation. This is basically what one expects intuitively: possible rapid emission of particles during the transit phase of the reaction followed by quasiequilibrium emission as the system separates, followed by statistical emission on a much longer time scale than the code has been run for here.

To summarize, we have established time scales for several processes which we expect to occur during the transit and separation phases of reactions at low and intermediate energies. From the computational point of view in particular, Figs. 2 and 4 show that the equilibration processes are largely complete by 250 fm/c after the reaction commenced, and it is not economical to continue evolving the reaction by this method beyond that time. Further, stopping the evolution at 150 fm/c is probably premature in that some of the reaction products may still be highly excited. Of course, this does not mean that the products are all in their ground states after 250 fm/c, an issue to which we will now turn.

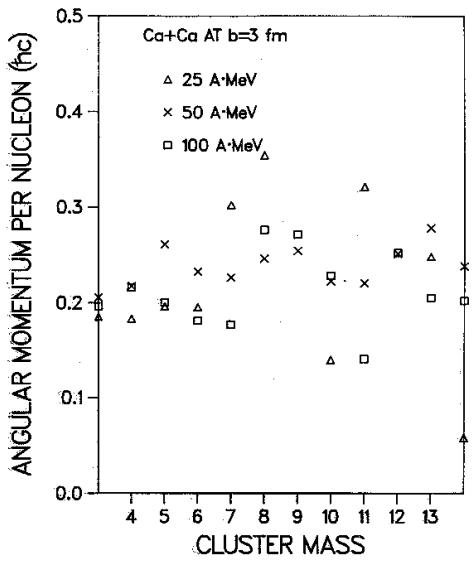

FIG. 6. Angular momentum per cluster for light fragments observed after an elapsed time of 250 fm/c for the reactions Ca+Ca at 25, 50, and 100A MeV and $b=3$ fm.

IV. EXCITATION ENERGIES

As was emphasized earlier, one of the advantages of the QPD approach is that the nuclear ground-state properties are given by the same Hamiltonian which is used to study their time evolution. This allows the calculation of excitation energies and, because the collision term conserves angular momentum, the spin distributions of reaction products. We begin with a discussion of the latter.

There is more energy deposited in the reaction region as the bombarding energy increases. Hence, one might expect that the fragments produced in higher-energy reactions would have greater average spin than those produced at lower energies. To investigate this possibility, we plot in Fig. 6 the angular momentum per nucleon for light clusters produced in the Ca+Ca reaction at 25, 50, and 100A MeV. The spins were determined after an elapsed reaction time of 250 fm/c. We do not find a particularly strong dependence of the angular momentum on either the impact parameter (not shown) or bombarding energy, even though the average kinetic energy of the clusters does increase with bombarding energy. We only claim this observation to be true at a time of 250 fm/c; once one includes the decays of excited states the conclusion may change. Whether final-state decays are important can be investigated by calculating excitation energies.

In order to calculate excitation energies, it is first necessary to construct a table of ground-state energies over the mass range of interest. This is a compute intensive task which can become quite onerous for heavy nuclei for two reasons: The valley of beta stability is increasing in width as the mass increases and the execution time for the simulation is increasing like the square of the mass number. The computational mass table which we have prepared thus far extends only up to mass 110, but is more than adequate for our purposes here. For each value of A, up to 15 isobaric nuclei are simulated, somewhat more heavily weighted to the neutron rich side.

For light fragments, the excitation energies basically follow the same behavior as is observed in Fig. 6 for the angular momenta, namely, that there is little dependence on impact parameter and bombarding energy. What is of greater interest is how much energy is left in the residual systems. This is shown in Figs. 7 and 8.

The results for Ca+Ca at 25A MeV and $b=0$ and 6 fm are shown in Fig. 7. For the peripheral collision, we would expect the lowest excitation energies to be found in systems close to $A=40$, and this is indeed observed. Nuclei with mass greater than 40 must be formed in few nucleon transfer reactions and would be expected to have a higher excitation energy, as is predicted by the simulation. In the central collision, a large system is formed. When this system has a mass equal to that of the combined projectile and target, its excitation energy must be equal to a quarter of the lab frame bombarding energy. This can be seen in Fig. 7 as well. Of course, such systems are not likely to be long lived, as was seen in Fig. 2, and they will lose excitation energy through particle emission. The trend shown in Fig. 7 is then what one expects for $b=0$: the excitation energy decreases with mass. The rate of change is 0.11 MeV per nucleon per mass unit, which, for a mass 70 system corresponds to 7.7 MeV. This is just what one expects on the basis of binding energy considerations.

Turning to the lower-energy Ar+C reaction at 12A MeV, one would expect less impact parameter dependence over much of its range, then substantial changes in excitation energy for peripheral collisions. This behavior can be seen in Fig. 8. There is not a large difference between the $b=2$ and 4 fm reactions, but $b=6$ fm is substantially different. For the peripheral reactions, far less

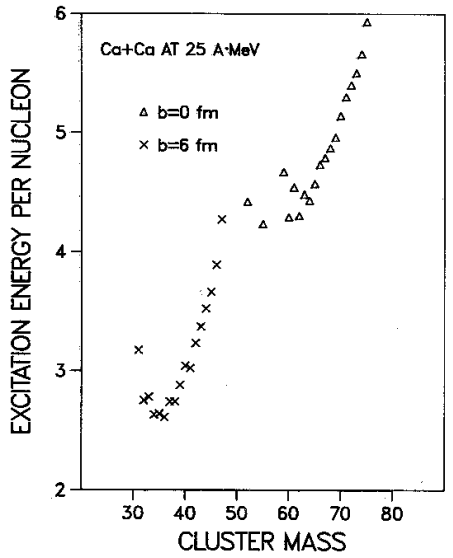

FIG. 7. Excitation energy per nucleon for heavy fragments emitted in the reaction Ca+Ca at 25 and $b = 0,6$ fm. The excitation energy is measured after a reaction time of 250 fm/c.

energy is deposited in the mass 40 system.

Also of interest is the distribution of excitation energies for a fixed fragment mass. Unfortunately, our limited statistics do not permit us to examine such distributions for a wide range of masses, and we are basically restricted to light systems and very heavy ones. For the Ca+Ca reactions, the distributions are shown in Fig. 9 for ^{4}He fragments as observed after an elapsed reaction time of 250 fm/c. Although it would be tempting to take the slope of this plot and extract a temperature from it, we were unable to do so since we have not determined the density of states for computational ^{4}He. However, there is some indication from both the average excitation energy and the relative slope that the fragments emitted in the central collision come from a more energetic system than do the ones emitted in the peripheral collision. Much better statistics will be needed to make this conclusion more quantitative.

Figs. 6 to 9 illustrate the necessity of including in the simulation a means of handling long time scale processes. The excitation energies obtained in the simulation of this reaction are moderate, of the order of several MeV per nucleon. Emission of particles from such a system are likely to involve barrier penetration effects and be on a much longer time scale than what the simulation is designed to handle efficiently. Hence, for these energy regions it is more appropriate to use the code to predict the excitation energy distributions of compound nuclei, and then use a statistically based code to follow the decays of these nuclei on the time frame of 10^4 fm/c.

One final topic which should be addressed before finishing this section is the impact parameter dependence of mass correlation functions. Correlations between the masses of pairs of fragments was shown using the SCEOM model[11] to have significant bombarding energy dependence for central collisions in the intermediate energy range. This change is associated with the transition from binary breakup through multifragmentation to va-

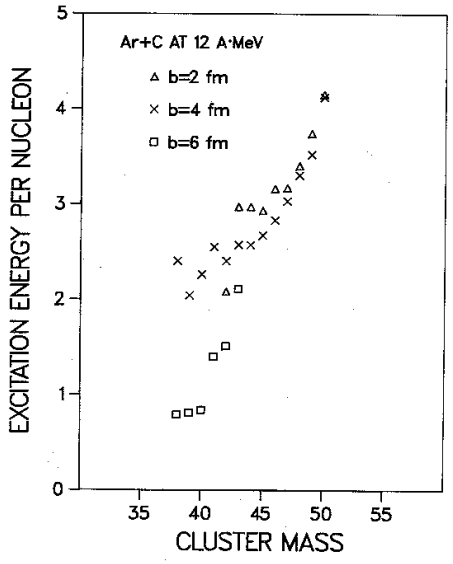

FIG. 8. Excitation energy per nucleon for heavy fragments emitted in the reaction Ar+C at 12A MeV per nucleon. The results are shown for three impact parameters: 2, 4, and 6 fm. The excitation energy is measured after a reaction time of 250 fm/c.

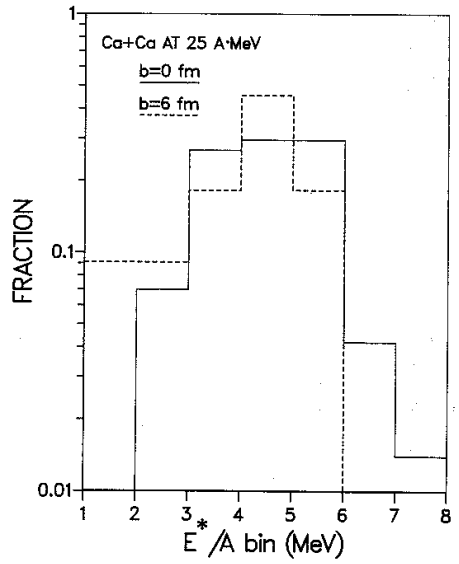

FIG. 9. Excitation energy per nucleon for He fragments emitted in the reactions of Fig. 2. The excitation energy is measured after an elapsed time of 250 fm/c.

porization. Because of the unstable ground-state problem of the SCEOM model, no attempt was made to investigate the variation of this correlation function with impact parameter. Depending on how an event trigger is selected for experiments to measure these correlations, knowledge of the impact parameter dependence is important.

We begin with a discussion of the pair probability distribution, rather than the correlation function. This is shown in Fig. 10 for the Ca+Ca reaction at 25A MeV for $b=0$ and 6 fm. The general features of the pair probability, as measured at 250 fm/c, are very different for the two impact parameters. In the peripheral collision, the most likely events are those in which two roughly equal mass nuclei are produced. In contrast, the central collision produces an excited system which will not decay totally by binary splits. However, it is clear that the impact parameter averaged data would show an enhancement along the binary split locus.

Further, it is also clear that a decay algorithm is going to be necessary in order to make a comparison with experiment. This can be illustrated by comparing the pair probability with the correlation function. The mass correlation function is constructed in the following manner. The correlation function $C(A_1, A_2)$ is defined by

$$C(A_1, A_2)=N_0\frac{N(A_1, A_2)}{N(A_1)N(A_2)}\ , \tag{11}$$

where $N(A_1, A_2)$ are the number of coincident pairs of fragments with mass A_1 and A_2, while $N(A)$ is the number of fragments with mass A. The constant N_0 normalizes the correlation function to unity. Because of the binning problems associated with the small samples available in computer simulations, we evaluate Eq. (11) by an event mixing technique whereby the number of true coincident pairs is divided by the number of pairs obtained by randomly selecting fragments from different events (appropriately normalized).

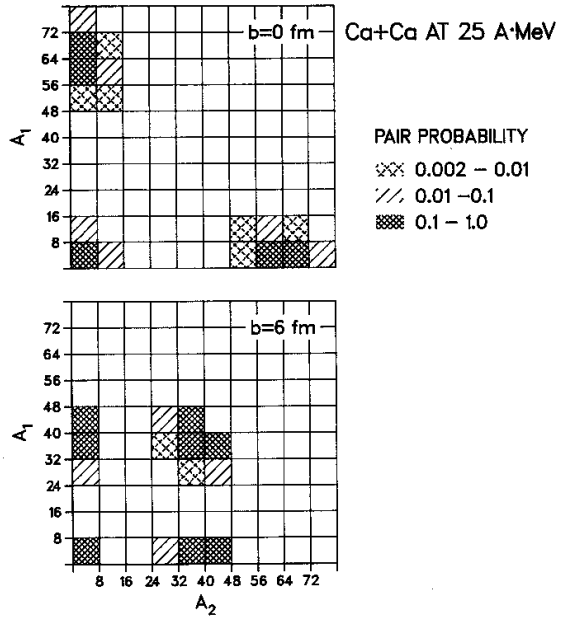

FIG. 10. Pair probability predicted for the Ca+Ca reaction at 25A MeV, and $b=0$ and 6 fm. The distribution was evaluated after an elapsed reaction time of 250 fm/c.

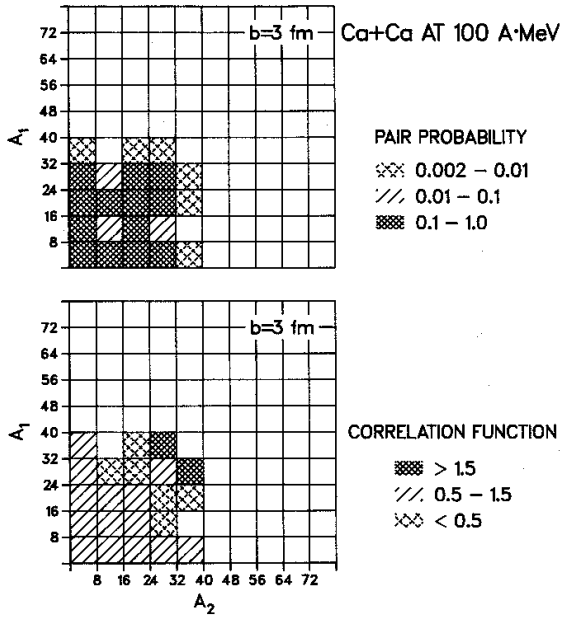

FIG. 11. Pair probability (top) and pair correlation function (bottom) shown for the reaction Ca+Ca at 100A MeV and $b=3$ fm. The distributions were determined after an elapsed reaction time of 250 fm/c.

In the absence of a decay scheme, we do not have sufficient events at 25A MeV to make a comparison between the pair probability and the correlation function. Hence, we choose to make the comparison at 100A MeV for $b=3$ fm. The results are shown in Fig. 11. At this bombarding energy, the collisions no longer lead to anywhere near the same number of binary splits as is observed at lower energies. The enhancement of the correlation function around $A_1\simeq A_2\simeq 35$ will very likely be reduced once the excitation energy has been decayed away and the pair probability is more uniform. This behavior emphasizes that care will have to exercised in using the mass correlations to investigate the liquid/vapor phase transition question.

V. CONCLUSION

A quasiparticle model[1] for computational nuclei based on a momentum dependent potential to represent antisymmetrization effects has been extended in this paper to include a collision term. We refer to the dynamical prescription for the model as quasiparticle dynamics or

QPD. The collision term is stochastic and yet conserves angular momentum as well as energy and linear momentum. The properties of this model then allow the prediction of excitation energy and angular momentum distributions of reaction products.

As a first application of the model, the characteristics of central collisions with high excitation energy are compared with those of peripheral collisions of low excitation energy. It is shown that many of intuitive features expected on the basis of the geometrical components of the reaction mechanism are borne out in the simulation. By examining the time evolution of the fragment mass distributions, as well as the nucleon emission rates, the natural reaction time scale of 250 fm/c can be established for the efficient use of the simulation. It is emphasized that for observables sensitive to processes with longer characteristic times (for example, compound nucleus decay) it is more efficient to couple the predictions of this model with one better based on the physics of such processes. Lastly, it is shown that certain observables such as the mass correlation function may have a strong impact parameter dependence. Measurements of such observables will not be easily interpretable without an event filter.

ACKNOWLEDGMENTS

This work was supported in part by the Natural Sciences and Engineering Research Council of Canada. We also wish to thank B. K. Jennings (TRIUMF) for helpful discussions.

[1]D. H. Boal and J. N. Glosli, Phys. Rev. C **38**, 1870 (1988).

[2]G. Bertsch, H. Kruse, and S. Das Gupta, Phys. Rev. C **29**, 673 (1984); for reviews, see D. H. Boal, Annu. Rev. Nucl. Part. Sci. **37**, 1 (1987); H. Stocker and W. Greiner, Phys. Rep. **137**, 277 (1986).

[3]L. W. Nordheim, Proc. R. Soc. London, Ser. A **119**, 689 (1928); E. A. Uehling and G. E. Uhlenbeck, Phys. Rev. **43**, 552 (1933).

[4]Particle Data Group, Lawrence Radiation Laboratory Report UCRL-200000NN, 1970.

[5]N. L. Balazs and B. K. Jennings, Phys. Rep. **104**, 347 (1984); M. Hillery, R. F. O'Connell, M. O. Scully, and E. P. Wigner, Phys. Rep. **106**, 121 (1984).

[6]G. E. Beauvais, D. H. Boal, and J. C. K. Wong, Phys. Rev. C **35**, 545 (1987).

[7]J. Aichelin and H. Stocker, Phys. Lett. **176**, 14 (1986).

[8]A. Vincentini, G. Jacucci, and V. R. Pandharipande, Phys. Rev. C **31**, 1783 (1985).

[9]This particular reaction is chosen since correlation data should be available soon from it. W. Benenson (private communication).

[10]J. R. Birkelund and J. R. Huizenga, Annu. Rev. Nucl. Part. Sci. **33**, 265 (1983).

[11]D. H. Boal and J. N. Glosli, Phys. Rev. C **37**, 91 (1988).